

Streamline Regularization for Large Discontinuous Motion of Sea Ice

M. Thomas¹, C. A. Geiger¹, P. Kannan² C. Kambhamettu¹

¹University of Delaware

²University of Pittsburgh

mani@udel.edu, cgeiger@udel.edu,

prk16@pitt.edu, chandrak@udel.edu

Abstract

Non-rigid motion has to sometimes contend with the presence of discontinuous structures when it is estimated under a non-topology preserving deformation. In this paper, we propose an algorithm that estimates large scale non-rigid motion in the presence of these discontinuous structures. We have developed a streamline regularization framework that uses particle streamlines to compute a plausible flow at discontinuities, thereby enabling us to predict the motion more accurately. To quantitatively validate the accuracy of our results, we applied the Wilcoxon Signed Rank Test, which shows an improvement in estimation accuracy using our proposed scheme.

1. Introduction

The polar extremes, especially the sea ice on the polar ocean surfaces serve as thermal regulators for the planet. The variable thickness and dynamic nature of the sea ice is intimately connected with the thermal regulation of planetary heat transfer between the air and oceans in the Polar Regions. Given the hostile nature of the Polar Regions, considerable manpower, instruments, and funding is required to accurately study the dynamics of sea ice. From an operational perspective, the discontinuous structures such as leads, slip lines, cracks, and ridges affect the mobility at a human scale, be it navigation or maintaining offshore structures [11]. It is thus very important to quantify the distribution, orientation and size of both continuous and discontinuous motion domains.

The problem of characterizing motion has been an area of active research in the sea ice community and the computer vision community. Within the former group, the problem of tracking sea ice has been addressed using a variety of methods including cross correlation [4] and 2D wavelets [8]. Most of the techniques estimate motion over a regular grid of estimation locations and

these grid points span continuous and discontinuous regions equally. In computer vision research, many techniques have been proposed and readers are directed to [5], and references therein for more information. Unfortunately, many of the proposed schemes are fine tuned to high frame rate cameras and do not address the kinds of problems that are present in remote sensed imagery. Typical displacements fall in the range of tens of pixels as described in [6]. In contrast, sea ice displacements are in the range of 100~200 pixels (with discontinuous structures in the range of 10s of pixels) due to the low image acquisition frequency (once in 1~3 days). Additionally, most of the available test data sets do not translate into a valid option to compare algorithms that are developed for satellite imagery.

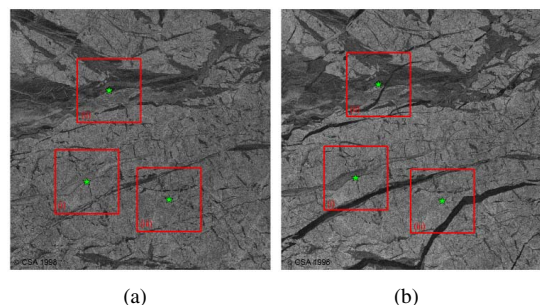


Figure 1. RadarSat-1 image pair showing discontinuous structures. The red boxes represent sample sections in the image while the green star depicts the collocated features in the image pair.

Figure 1 shows an example from a RadarSat-1 image pair collected during the SHEBA ice camp [9] where changes in the backscatter signature caused by geophysical changes in the structures between image pairs are evident. This image pair highlights the difficulties that are encountered when handling the large magnitude motion and the large discontinuous structures. Given the typical structures observed in sea ice, a model that

tracks motion despite the presence of large discontinuities would be valuable for researchers. This model would be especially useful in studying structural failure and a possible initialization point for physics-based numerical models. In this work, we demonstrate a motion tracking model that uses an Expectation Maximization (EM) framework to estimate motion at close proximity to discontinuities. We specifically demonstrate the reliability of this framework using remote sensed data of sea ice, but it will be evident that this method easily generalizes to other kinds of imagery also.

We begin this paper with a brief overview of our algorithm, and then go on to analyze the performance of our algorithm with real data sets containing large discontinuous motion. We finally conclude our work with possible extensions and improvements.

2. Streamline Regularization

We have based our algorithm on two different research works. Our motion tracking system was built on the work by Thomas et al. [10], where the authors described a cascaded scheme to tackle the large motion encountered in sea ice. The second work was by Bertalmio et al. [1] on image inpainting, where defects in images are replaced by intelligently propagating structural and textural information from neighboring pixels.

Here, we propose an iterative EM-like algorithm to track motion at discontinuous locations. The “E” step propagates flow from adjacent continuous regions into discontinuities while the “M” step validates the flow by computing the motion from the image pair. In the cascaded motion estimation scheme [10], the authors used a median based filtering scheme (an isotropic regularizer) to enforce smoothness constraints.

In our work, we segment the motion field into continuous and discontinuous zones using the total deformation of the motion field [7]. We enforce isotropic smoothness constraints in the continuous zones but propagate the flow from adjacent continuous regions to “inpaint” the discontinuous locations.

2.1. Direction Estimation

The propagation of flow into discontinuous locations can be decomposed into two stages. The first stage estimates the ideal direction, while the second stage uses these results to compute the magnitude of the output vector. To compute the orientation, we computed the local polynomial approximations to a streamline using the Line Integral Convolution (LIC) algorithm proposed by Lee and Cabral [3]. Figure 2 shows the discontinuous

locations (green circles) and the 3rd order polynomial approximations (dashed lines) for a few sample streamlines.

Since all the streamlines were approximated using parametric polynomials, the local tangential direction is computed as $\arctan(y'(s)/x'(s))$, where $y(s)$ and $x(s)$ are the explicit polynomial approximations using arc length parameterization. The best direction (\mathbf{e} in algorithm 1) is computed as the maximum a posteriori (MAP) estimate of local orientations within the estimation neighborhood.

2.2. Magnitude Estimation

To estimate the magnitude of motion, vectors (shown as dark red arrows in Fig. 2b) that are highly correlated ($\leq \theta_0$) to the estimated orientation are extracted as potential contributors. The final vector magnitude ($\|\mathbf{v}\|$ in algorithm 1) is computed by solving a scattered data interpolation problem using Radial Basis Function [2] over the potential vectors.

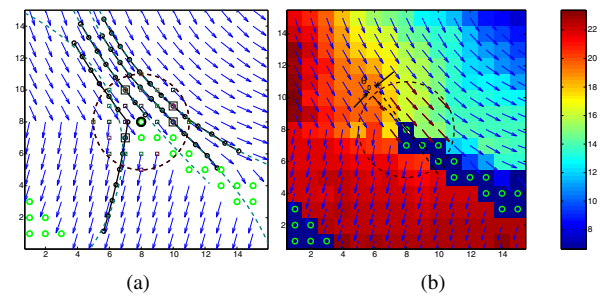


Figure 2. (a) Extrapolated polynomials as an estimate of the streamline trajectory (b) Interpolation of magnitude using Radial Basis Functions. The green circles represent the discontinuous locations while the blue arrows represent the motion in the continuous regions.

The final estimate ($\mathbf{v} = \|\mathbf{v}\|\mathbf{e}$ in algorithm 1) is used to replace the original value at the discontinuous grid location. This process is repeated over all the discontinuous grid locations in an “onion-peel” fashion, working our way from the outside (the locations of a discontinuity that are adjacent the continuous regions) towards the inside (central portion of a discontinuity). Once all the estimates are computed (E-step), the image pair is used to validate the estimated vectors (M-step). This entire process is repeated at each estimation node in the cascade scheme to recover an accurate estimate of motion in the continuous and discontinuous locations.

An overview of our scheme is provided in algorithm 1. The readers are urged to note that the Forward (+) and Backward (-) steps require two sequential loops, but for succinctness, they were combined into a single loop.

Algorithm 1 Streamline regularization at a grid location

Require: $\mathbf{u} \in \mathbb{R}^{h \times w \times 2}$
 $\mathbf{e}^{ij} \leftarrow \mathbf{u}^{ij} / \|\mathbf{u}^{ij}\|, i = 1 \dots h, j = 1 \dots w$
 $x_0 \leftarrow \lfloor w/2 \rfloor, y_0 \leftarrow \lfloor h/2 \rfloor$
for all (r, c) such that $r = 1 \dots h, c = 1 \dots w$ **do**
 if $\sqrt{(r - y_0)^2 + (c - x_0)^2} \leq \mathcal{R}$ **then**
 $x = c, X \leftarrow [x], y = r, Y \leftarrow [y], S \leftarrow [0]$
 {+ Forward, - Backward}
 for $k = 1$ to $\mathcal{L}/2$ **do**
 $(x, y) \leftarrow (x, y) \pm \mathbf{e}^{\lfloor \text{round}(x), \text{round}(y) \rfloor}$
 if $x = \phi$ or $y = \phi$ **then**
 break $\{(x, y)$ marked for regularization $\}$
 end if
 {Append values into X, Y and S }
 $X \leftarrow [X, x], Y \leftarrow [Y, y]$
 $S \leftarrow [S, \pm \sqrt{(x - c)^2 + (y - r)^2}]$
 end for
 Fit polynomials $X(S)$ and $Y(S)$
 Extrapolate polynomials, $X(S)$ and $Y(S)$
 end if
 $e = \text{MAP estimate} [\arctan(Y'(S)/X'(S))]$
 $\|\mathbf{v}\| = \text{RBF interpolation using } \mathbf{e}$
 Output: $\mathbf{v} = \|\mathbf{v}\|\mathbf{e}$
end for

3. Results and Analysis

To observe the accuracy of the algorithm at discontinuities, we have used both qualitative and quantitative analyses. For the qualitative studies, we have compared our algorithm against the estimates from [10]. Figure 3 shows highlighted sections in Fig. 1 after the two algorithms (isotropic regularization from [10] and streamline regularization (described in this paper) were applied to the sample image pairs. The first row in Fig. 3 shows the results obtained using isotropic regularization, while the third row shows the results obtained using the streamline method. The second and fourth rows are absolute intensity differences between the first image and the warped second image, where the warping used the motion from the isotropic and streamline methods, respectively. The color bar for the error maps are scaled to represent the same maximum value, wherein blue indicates smaller error. As can be seen, isotropic regularization performs well in continuous re-

gions while streamline regularization performs equally well in both continuous and discontinuous regions.

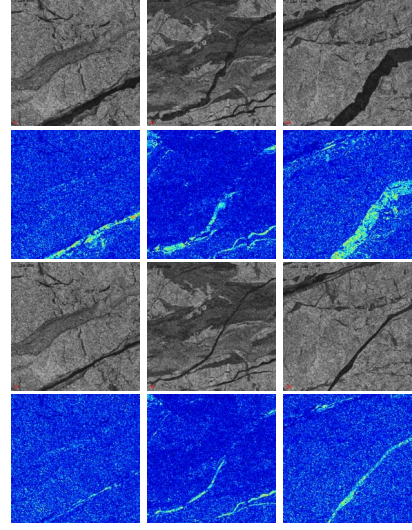


Figure 3. Comparison of the error metrics for the image pairs in Fig. 1. The first and third rows represent warped images while the second and fourth rows depict the absolute intensity difference obtained by the isotropic and streamline regularization, respectively.

In order to quantitatively establish the robustness of the streamline regularization, we separately estimated motion for 12 different image pairs using the isotropic and streamline regularization algorithms. We then randomly sampled 120 locations along discontinuous boundaries and used these locations to sample 100x100 pixel regions from the first image and the motion warped second image. The mean absolute intensity difference was measured for the 120 samples obtained from the two algorithms.

The null hypothesis stated that there was no significant variation between the two algorithms. The alternate hypothesis stated that the streamline regularizer produced lower errors. The differences in the mean intensity differences produced by the two algorithms were rank ordered and the Wilcoxon Signed Rank test [12] was used to evaluate the data at $\alpha = 0.01$. In this case, we resorted to a non-parametric test because the samples chosen from discontinuous regions, and are not necessarily modeled from a normal distribution. Unlike a parametric repeated measures t -test, the Wilcoxon Signed Rank test does not make any assumptions about normality.

The reduction in estimated errors using the stream-

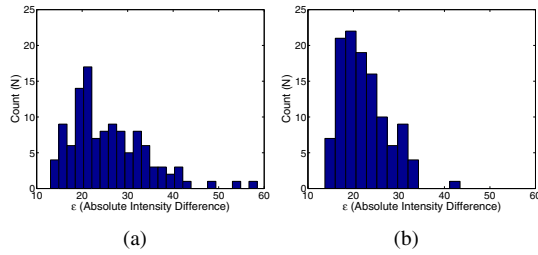


Figure 4. Pixel error distributions for 120 samples from 12 image pairs for discontinuous locations using (a) Isotropic regularization (b) Streamline regularization. The x-axis represents the mean absolute intensity difference.

line algorithm can be observed in Fig. 4, which depicts the error distributions as a histogram. In the figures, the improvement using the streamline algorithm is evident with a larger number of data points clustered towards the left in panel (b) when compared to panel (a). Furthermore, the Wilcoxon test results show a significant reduction in errors when using the streamline regularization ($W = 4240, p < 0.001$). Since alpha was set at $p < 0.01$, any obtained probability less than 1% would lead to a rejection of the null hypothesis. It can therefore be concluded that the streamline algorithm would produce significantly smaller errors that can be generalized beyond our sample of 120 locations.

4. Conclusion

This paper attempts to provide a mechanism for estimating motion at close proximity to discontinuous zones. Typical methods face problems when attempting to characterize motion at these locations due to the failure of any mathematical model to describe the process. Reduction in the uncertainty in estimating the location and motion near these damage zones would be very valuable for researchers involved in the study of crack propagation and structural failures. This could also be a useful initialization for physics-based numerical sea ice models that study the characteristics of these discontinuities. In this work, we propose a streamline regularization scheme to handle discontinuities where the vector fields were iteratively readjusted based on estimates from continuous neighborhoods. From the results, we can see that the error rate is significantly lower for the streamline algorithm, when compared to the isotropic regularization. One of our future directions is to incorporate this framework into a variational model to study higher order motion models.

5. Acknowledgments

This work is supported through grants from NSF Arctic Natural Science within the Office of Polar Programs (ARC-0612105). The SAR imagery was provided through the Alaska Satellite Facility through agreements with the ©Canadian Space Agency (1997) and NASA for RadarSat-1 imagery.

References

- [1] M. Bertalmio, G. Sapiro, V. Caselles, and C. Ballester. Image inpainting. In *SIGGraph-2000*, pages 417–424, 2000.
- [2] F. Bookstein. Principal warps: Thin-plate splines and the decomposition of deformations. *PAMI*, 11(6):567–585, June 1989.
- [3] B. Cabral and L. C. Leedom. Imaging vector fields using line integral convolution. In *Proc. of 20th conference on Comp. graphics and interactive tech.*, pages 263–270, 1993.
- [4] M. Drinkwater. *Analysis of SAR Data of the Polar Oceans*, chapter Satellite microwave radar observations of Antarctic sea ice, pages 145–187. Springer-Verlag, 1998.
- [5] D. J. Fleet and Y. Weiss. *Handbook of Mathematical Models in Computer Vision*, chapter Optical Flow Estimation. Springer, 2005.
- [6] M. Gong and Y. H. Yang. Estimate large motions using the reliability-based motion estimation algorithm. *Int. J. Comput. Vision*, 68(3):319–330, 2006.
- [7] R. W. Lindsay, J. Zhang, and D. A. Rothrock. Sea ice deformation rates from measurements and in a model. *Atmosphere-Oceans*, 40:35–47, 2003.
- [8] A. K. Liu and D. J. Cavalieri. On sea-ice drift from the wavelet analysis of the defense meteorological satellite program (DMSP) special sensor microwave imager (SSM/I) data. *Int. J. Remote Sens.*, 19(7):1415–1423, 1998.
- [9] H. L. Stern and R. E. Moritz. Sea ice kinematics and surface properties from radarsat synthetic aperture radar during the sheba drift. *J. Geophys. Res.*, 107(C10), 2002.
- [10] M. Thomas, C. A. Geiger, and C. Kambhamettu. High resolution motion estimation of sea ice using an implicit quad-tree approach. In *ISPRS Workshop on High-Resolution Earth Imaging for Geospatial Information*, May 2007.
- [11] M. Thomas, C. A. Geiger, C. Kambhamettu, J. Hutchings, and M. Engram. Near real time application of SAR-derived sea ice differential motion during APLIS ice camp 2007. In *RSP Society Annual Conference*, September 2007.
- [12] F. Wilcoxon, S. Katti, and R. A. Wilcox. *Critical values and probability levels for the Wilcoxon Rank-Sum test and the Wilcoxon Signed-Ranks test*. American Cyanamid Company, Wayne, NJ, 1963.